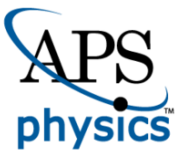

This is the accepted manuscript made available via CHORUS. The article has been published as:

Quantum Interferometry with a g-Factor-Tunable Spin Qubit

K. Ono, S. N. Shevchenko, T. Mori, S. Moriyama, and Franco Nori

Phys. Rev. Lett. **122**, 207703 — Published 24 May 2019

DOI: 10.1103/PhysRevLett.122.207703

Quantum interferometry with a g-factor-tunable spin qubit

K. Ono[1,2], S. N. Shevchenko[3,4,5], T. Mori[6], S. Moriyama[7], Franco Nori[3,8]
[1] *Advanced device laboratory, RIKEN, Wako-shi, Saitama 351-0198, Japan*
[2] *CEMS, RIKEN, Wako-shi, Saitama 351-0198, Japan*
[3] *Theoretical Quantum Physics Laboratory, RIKEN Cluster for Pioneering Research, Wako-shi, Saitama 351-0198, Japan*
[4] *B. Verkin Institute for Low Temperature Physics and Engineering, Kharkov 61103, Ukraine*
[5] *V. N. Karazin Kharkov National University, Kharkov 61022, Ukraine*
[6] *Nanoelectronics Research Institute, National Institute of Advanced Industrial Science and Technology (AIST), Tsukuba, Ibaraki 305-8568, Japan*
[7] *International Center for Materials Nanoarchitectonics, National Institute for Materials Science (NIMS), Tsukuba, Ibaraki 305-0044, Japan and*
[8] *Department of Physics, The University of Michigan, Ann Arbor, MI 48109-1040, USA*
(Dated: April 20, 2019)

We study quantum interference effects of a qubit whose energy levels are continuously modulated. The qubit is formed by an impurity electron spin in a silicon tunneling field-effect transistor, and it is read out by spin blockade in a double-dot configuration. The qubit energy levels are modulated via its gate-voltage-dependent g-factors, with either rectangular, sinusoidal, or ramp radio-frequency waves. The energy-modulated qubit is probed by the electron spin resonance. Our results demonstrate the potential of spin qubit interferometry implemented in a silicon device and operated at a relatively high temperature.

PACS numbers: 73.63.Kv, 73.23.Hk, 76.30.-v

Introduction.—Sensitive measurement techniques are based on the interference of waves. The most striking illustration is the recent use of interferometry for the detection of gravitational waves [1]. If in place of classical electromagnetic waves one can use the wave functions of quantum objects, such techniques can be called quantum interferometry. This was studied not only for conventional small quantum objects [2, 3], but also for large organic molecules [4, 5] and micrometer-size superconducting circuits [6–8]; see also a recent review article [9] for different realizations and applications in quantum sensing. Since it is difficult to maintain a coherent superposition of charge states, it might be more beneficial to use instead the spin degree of freedom [10]. Interestingly, silicon, the second most abundant element in the Earth's crust and the base of modern electronics, is an ideal environment for spins in the solid state [11]. In this work, we will explore how to use a single-spin silicon-based qubit for quantum interferometry.

Among other characteristics, for quantum engineering it is important to have qubits which are "hot, dense, and coherent" [12]. In this context, "hot" means working in the technologically less challenging few-Kelvin regime rather than being cooled down to the milli-Kelvin domain. "Dense" refers to the possibility to achieve high density of quantum dots or donors in semiconductors. Another benefit of this platform is its compatibility with the well-developed complementary-metal-oxide-semiconductor (CMOS) technology. Even more, it has been shown [13–15] that transistors can behave as quantum dots, in which either charge or spin qubits are realized.

Quantum systems can be modulated by signals of different shapes, such as sinusoidal and square-wave signals. The latter allows one to rapidly change a qubit state from one to another, which we can refer to as latching modulation of qubit states [16, 17]. If this is done with a period longer than the coherence time, then the response has two separate peaks, situated at the two resonance frequencies corresponding to the two states. Increasing the modulation frequency, the coherent response is displayed as an averaged signal, situated at a frequency between the two resonance frequencies mentioned above, which is known as motional narrowing. Both motional averaging and narrowing are known in NMR systems and recently also studied in superconducting systems [18, 19]. In this way, by changing the modulation frequency, namely its ratio to the coherence rate, one can observe the transition between classical (incoherent) and quantum (coherent) regimes, as in Refs. [18, 20–22].

In this work, we focus on the time-ensemble behavior of a spin-1/2 qubit and study the effect of continuously modulating the qubit energy. In this way, we explore the motional averaging not only for the symmetric latching modulation (which was previously demonstrated in superconducting qubits [16–18]), but also in the asymmetric regime, where dwelling in one state is longer than in the other state. A square-wave modulation with variable duty ratio shows weighted motional averaging. At low modulation frequency, this is visualized, in the frequency dependence, by two peaks (with weighted height and width); while at high modulation frequency there is only one averaged peak. We also demonstrate the sinusoidal energy modulation of the spin qubit and show the Landau-Zener-Stückelberg-Majorana (LZSM) interference of the spin resonance signal. This is the first demonstration of LZSM interference where the temperature is much higher than the photon energy of the sinusoidal modulation frequency. For realizations of the low-temperature LZSM interference in quantum-dot sys-

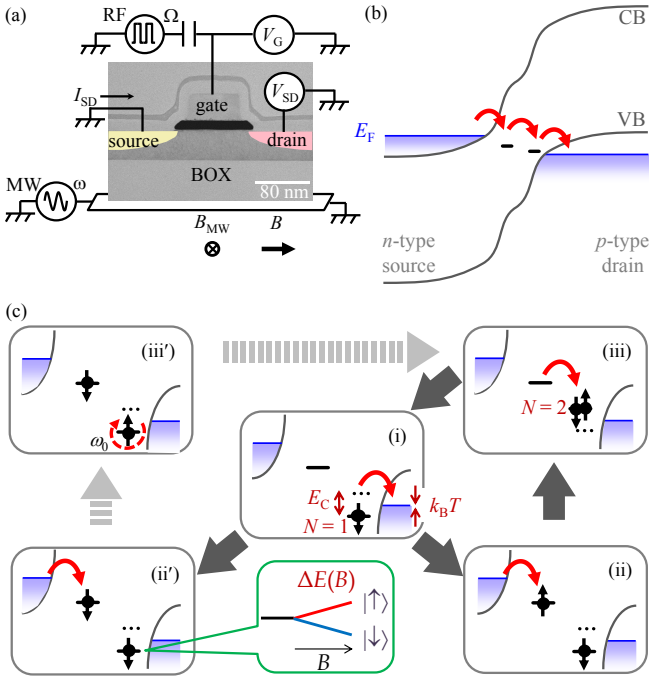

FIG. 1: **High-temperature TFET-based single-spin qubit.** (a) Schematic of the device and measurement set up. The transistor is defined on a SOI structure with n-type source and p-type drain electrodes. The channel length and width are 80 nm and 10 μm, respectively. The source-drain current I_{SD} of the device is measured for the source-drain voltage V_{SD}; and the gate voltage V_G at temperature $T = 1.6$ K is achieved with a pumped ^{4}He cryostat. A magnetic field B is directed along the source-drain current. A microwave (MW) signal is applied on the substrate. A gate-voltage modulation in the MHz regime is applied through a high-pass block capacitor with cutoff frequency (< 10 kHz) much smaller than the modulation frequency ($\sim$MHz). (b) Schematic of the potential landscape of the device. (c) Schematic of the single-electron tunneling cycle in the spin-blockade regime; see the SM for details.

tems see Refs. [23–30].

Device and measurement.—We used a spin qubit device based on a short-channel tunneling field-effect transistor, TFET [31], with the implanted deep impurity, Fig. 1(a) [32–36]. The device is essentially a gate-tunable PIN diode (a diode with an undoped intrinsic semiconductor region between a p-type semiconductor and an n-type semiconductor region). The ion implantations created coupled Al-N impurity pairs in silicon [37–40]. For an appropriate channel length, a three-step tunneling from the n-type source electrode to the p-type drain electrode occurs via two localized states in the channel, Fig. 1(b). The PIN structure allows tunneling via the localized states of a deep impurity and a shallow impurity [36, 41].

Spin blockade and ESR.—The device has two localized states, which behave as a double quantum dot device, where the current is defined by single-electron transport [42]. Under an appropriate source voltage V_{SD} and gate voltage V_G, the device shows spin blockade (SB) [43]. At the electron spin resonance (ESR) for one of the spins in the double dot, the source-drain current I_{SD} increases due to the lifting of the spin blockade Fig. 1(c) [13, 44]. Note that the large on-site Coulomb energy and strong confinement of these impurities allow a spin-qubit operation with a reasonable coherence time ($T_2^* = 0.2-0.3$ μs) at relatively high temperatures and low magnetic fields [45]. Changing the gate voltage V_G within the spin blockade region changes the g-factor by about 1% due to the Stark effect [46].

We describe our spin qubit device as a two-level system with the pseudo-spin Hamiltonian $H(t) = B_z(t)\sigma_z/2 + B_x(t)\sigma_x/2$. The longitudinal part is defined by the Zeeman splitting, $B_z(t) = g(t)\mu_B B$. The time-dependent gate voltage changes the g-factor by a small value and we have $B_z/\hbar = \omega_0 + \delta \cdot s(t)$, where the amplitude $\delta \ll \omega_0$; $\omega_0 = 2\pi f_0$ represents the ESR frequency. In this work, we consider three types of signals [41]: a sinusoidal modulation, $s(t) = \cos\Omega t$, a latching modulation, given by

$$s(t) = \begin{cases} 2d, & 0 < \Omega t/2\pi < 1-d, \\ -2(1-d), & 1-d < \Omega t/2\pi < 1, \end{cases} \quad (1)$$

where d is the duty-cycle ratio, and a ramp modulation, given by the fractional part in $\{\Omega t/2\pi\}$. Note that for a symmetric latching modulation, with $d = 1/2$, from Eq. (1), we have $s(t) = \mathrm{sgn}(\cos\Omega t)$. In addition, the transverse part of the Hamiltonian is defined by the MW voltage applied to the substrate, $B_x/\hbar = 2G\cos\omega t$ with amplitude G and circular frequency $\omega = 2\pi f$. The modulation is assumed to be slow, i.e. $\Omega \ll \omega$.

Square-wave modulation.—In figures 2 and 3 we present the results of our measurements and calculations for symmetric and asymmetric square-wave modulation signals. The left panel focuses on the source-drain current I_{SD}, showing the current derivative, dI_{SD}/df, in its main panel. The right panel presents the corresponding theoretical predictions for the qubit upper-level occupation.

By adding a square-wave MHz modulation signal to the gate [Fig. 2(a)], the gate voltage, i.e. g-factor, can be switched between two values, as described by Eq. (1). Figure 2(d) shows I_{SD} at $V_G = -0.36$ V and square wave of frequency 0.5 MHz and amplitude 32 mV. Due to the slow measurement with a time constant (that shows how fast the measured current changes) ~ 0.3 s, we observe the two ESR peaks with two different g-factors for $V_G = -0.36 + 0.016$ V and $-0.36 - 0.016$ V, respectively. By increasing the modulation frequency, the ESR peaks show a characteristic interference pattern and eventually a strong (main) peak appears with weak sideband peaks [Fig. 2(b)]. The strong single peak at $f = f_0 = 9.01$ GHz [Fig. 2(b)] is a result of motional averaging of the two peaks for the slow modulation [Fig. 2(d)]. A similar pattern was observed for latching modulation of the energy of a superconducting qubit in Ref. [16]. Changing the modulation amplitude shows a similar behavior with

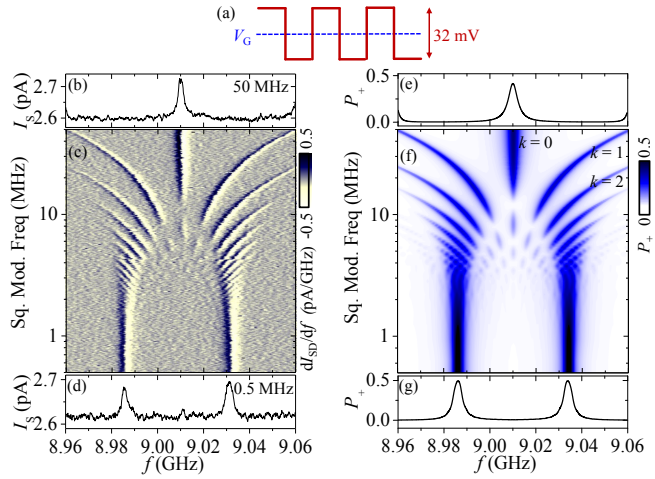

FIG. 2: **Square wave modulation of the spin qubit.** (a) Shape of the rf signal. (b,c,d) The source-drain current I_{SD} of the device with a square modulation of its full amplitude 32 mV added to the gate at $V_G = -0.36$ V through the high-pass block capacitor. Other conditions are the same as in Fig. 1. In panel (c) we present the intensity plot of dI_{SD}/df versus the frequency f and the square-wave modulation frequency Ω (log scale from 0.5 to 50 MHz), showing the evolution from the two ESR peaks into the strong main ESR peak and weak sideband peaks. Note that the distance between the main and the sideband peaks (seen in the upper area > 10 MHz) is linear in the modulation frequency Ω. Panels (b) and (d) present the source drain current I_{SD} at modulation frequencies of 50 MHz and 5 MHz, respectively. (e,f,g) Calculation of the upper-state population of the qubit under square-wave modulation of its energy. For calculations, the following parameters were used for all the graphs: $G/2\pi = 1.1$ MHz, $\Gamma_1/2\pi = 0.2$ MHz, $\Gamma_2/2\pi = 1$ MHz, and also for the right panels (e-g) here: $\delta/2\pi = 24$ MHz.

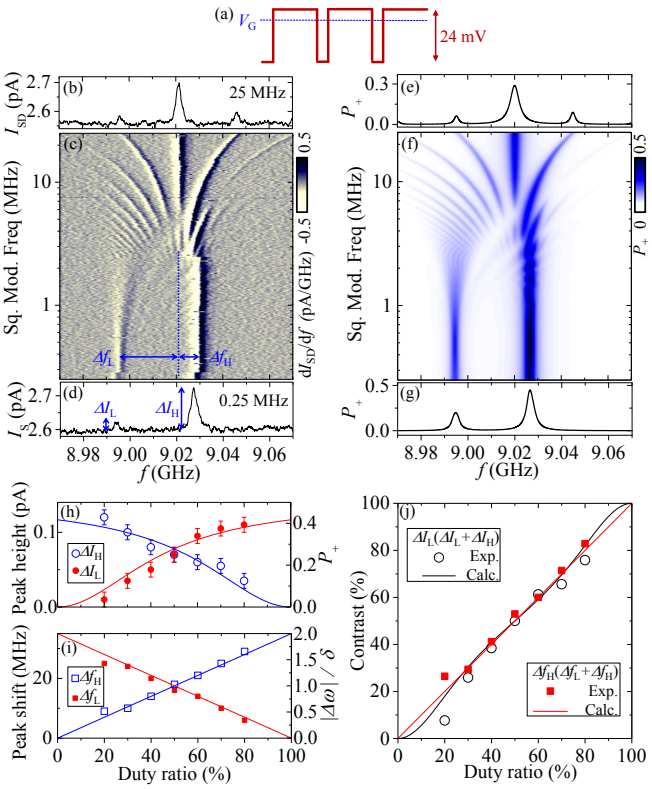

FIG. 3: **Weighted averaging for the spin qubit versus the duty ratio d.** (a) Shape of a square wave with $d = 20\%$. (b-d) Similar plot of I_{SD} as in Fig. 2(b-d) but with a square wave with a 20% duty ratio, which corresponds to $d = 0.2$. The modulation frequency is changed from 0.25 to 25 MHz in a log scale. (e-g) Calculation of the qubit upper-state population under square-wave modulation ($d = 0.2$) of its energy. Besides the duty ratio, other parameters are the same as in Fig. 2(e-g). Note that the main weighted averaged peak appears again at $f = f_0$ (here $f_0 = 9.02$ GHz), independent of the duty ratio. (h) Duty ratio dependence of the ESR peak heights at $\Omega/2\pi = 0.25$ MHz for lower frequency, ΔI_L, and higher frequency, ΔI_H. The ΔI_L and ΔI_H for $d = 0.2$ are indicated in (d). (i) The duty-ratio dependence among three ESR peaks, i.e. the motional averaged main peak at $\Omega/2\pi = 25$ MHz (9.021 GHz), to the ESR peaks of lower/higher frequency at $\Omega/2\pi = 0.25$ MHz. The distances between the peaks, Δf_L and Δf_H, are indicated in (e) for $d = 0.2$. (j) Duty-ratio dependence of the contrasts for the peak heights and distances.

a similar crossover frequency [41].

In order to describe the system, we solve the Bloch equations with the above Hamiltonian. We assume that $\omega \gg \Omega$ and after a rotating-wave approximation

$$H_1 = \frac{\hbar}{2}\left[\Delta\omega + \delta\cdot s(t)\right]\sigma_z + \frac{\hbar G}{2}\sigma_x, \qquad (2)$$

where $\Delta\omega = \omega_0 - \omega = 2\pi\left(f_0 - f\right)$. Details of the calculations are presented in [41], cf. Refs. [47, 48]. As a result, the upper-level occupation probability is readily obtained from the stationary solution of the Bloch equations:

$$P_+\left(\Delta\omega, \frac{\delta}{\Omega}\right) = \frac{1}{2}\sum_{k=-\infty}^{\infty}\frac{G_k^2(\delta/\Omega)}{G_k^2(\delta/\Omega) + \frac{\Gamma_1}{\Gamma_2}\left(\Delta\omega - k\Omega\right)^2 + \Gamma_1\Gamma_2}, \qquad (3)$$

where $G_k(x) = G\left|\Delta_k(x)\right|$, which can be interpreted as the dressed qubit gap, modulated by the function $\Delta_k(x)$. The relaxation and decoherence rates are denoted as $\Gamma_1 = T_1^{-1}$ and $\Gamma_2 = T_2^{-1}$, respectively. In particular, for rectangular modulating system with duty-cycle ratio d, we obtain:

$$\left|\Delta_k(x)\right| = \frac{2}{\pi}\frac{x\sin\left[\pi\left(1-d\right)\left(k-2dx\right)\right]}{\left(k+2\left(1-d\right)x\right)\left(k-2dx\right)}. \qquad (4)$$

We can interpret the effective Hamiltonian (2) as follows. The microwave drive dresses the two-level system resulting in an energy level difference $\Delta\omega$; when this is matched to the k-photon energy of the rf-signal, the dressed qubit is resonantly excited. Indeed, the upper-level population in Eq. (3) has maxima at $|\Delta\omega| = k\Omega$

[18, 49]. With Eq. (3) we generated the interferograms in the right panels of Figs. 2-4. [41] In particular, for Fig. 2 we used Eq. (4) with $d = 1/2$.

Asymmetric modulation.—Changing the duty ratio d (ratio of the low V_G signal duration to the period; for the previous square wave the duty ratio was 50%), shows both asymmetric modulation and weighted motional average, as demonstrated in Fig. 3. Because the modulation voltage is added through the block capacitor, the areas of the signal curves below and above the average gate voltage V_G are equal, as shown in Fig. 3(a). Figure 3(d) shows the ESR under slow modulation of the square-wave signal with a 20% duty ratio. The two ESR peak heights are different, reflecting the duty ratio. For fast modulation, the main peak appears at the weighted averaged frequency [Fig. 3(b)].

We repeat similar measurements with various duty ratios (from 20 to 80%). In figure 3(h) we plot the heights of the two ESR peaks at lowest modulation frequency. For each duty ratio, we also plot distances between the above two peak positions and the motional averaged main peak position at the highest modulation frequency [Fig. 3(i)]. Both of the peak heights and distances reflect the duty ratios. The ratio of the peak heights and the frequency distances are plotted in Fig. 3(j), and show the motional-averaged main peaks, which indeed appear at the weighted average frequency. The deviations from linear dependencies in these plots, especially for the duty ratio of 20%, are due to the gate-voltage dependence of the ESR peak height. More detailed measurements for each duty ratio are shown in [41].

We note here the following interesting features of the weighted motional averaging. The rectangular-pulse modulation places the qubit in one of the two allowed positions, and the low-frequency characteristics reflect the weighted time spent in those two states. For high Ω, the principal ESR line is situated in-between the two qubit states, the position of which is independent of the duty ratio. A counter-intuitive aspect is that the position of this line does not relate to any of the two qubit states, and thus is referred to as "motional averaging" [18]. Details of calculations are presented in [41]. There, it is shown that the frequency shifts are the following: $\Delta f_{\rm L} = -2d\delta$ and $\Delta f_{\rm H} = 2(1-d)\delta$, while the peak heights are nonlinear functions of d. These formulas are plotted with solid lines in Fig. 3(h-j).

Sinusoidal and ramp modulation.—Figure 4(b,c) shows the effect of the sinusoidal modulation that produces the Landau-Zener-Stückelberg-Majorana interference patten. The modulation amplitude dependence with fixed modulation frequency shows the radio-frequency-wave assisted side bands [41]. In the case of a sinusoidal modulation, the dressed energy gap is given by the Bessel function of the first kind $\Delta_k(x) = J_k(x)$.[49] Then, with Eq. (3) we plot Fig. 4(c). Ramp-wave modulations are shown in Fig. 4(e,f). An inverse ramp waveform gives identical results [41]. We note that at low modulation frequency Ω and low detuning $\Delta\omega$ the agreement is rather

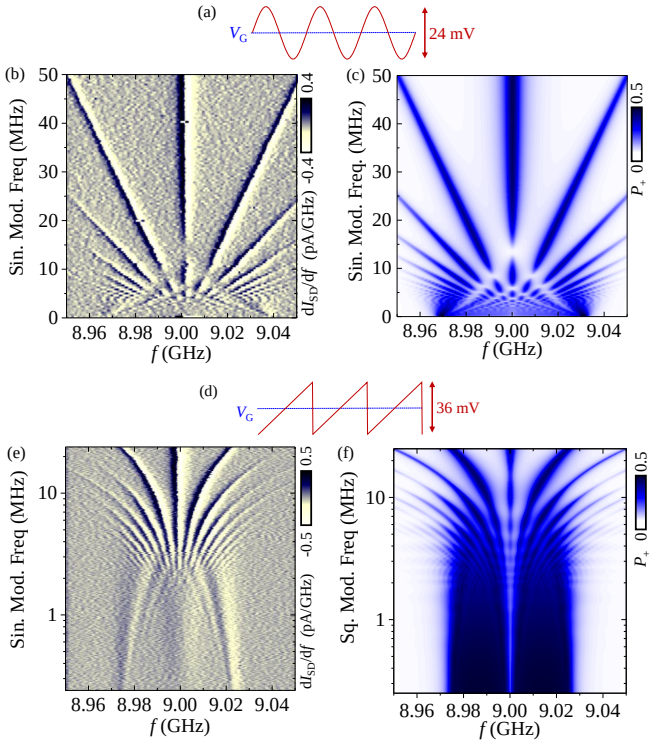

FIG. 4: **Sinusoidal and ramp modulation.** (a) Shape of the rf sinusoidal signal. (b) Source-drain current I_{SD} under sinusoidal modulation with amplitude 24 mV. Intensity plot of dI_{SD}/df versus the frequency f and the modulation frequency Ω (linear scale from 0 to 80 MHz). (c) Calculation of the upper-state population of the qubit under the sinusoidal modulation of its energy. The parameters are the same as for Fig. 2 besides the amplitude, which here is $\delta/2\pi = 30$ MHz. (d) Shape of the ramp wave signal. (e) Source-drain current I_{SD} under the ramp modulation with amplitude 36 mV. Intensity plot of dI_{SD}/df as a function of the frequency f and the modulation frequency Ω (log scale from 0.25 to 25 MHz). (f) Calculation of the upper-state population of the qubit under ramp modulation of its energy. The parameters are the same as for Fig. 2 besides the amplitude, which here is $\delta/2\pi = 27$ MHz.

qualitative, which might be due to the rotating-wave approximation.

Discussion.—We have demonstrated that under certain conditions, an impurity in a field-effect transistor behaves as a single-spin qubit which displays coherent phenomena, such as Landau-Zener-Stückelberg-Majorana interference and motional averaging. The spin-qubit device is based on a short-channel TFET in which, for an appropriate channel length, a three-step tunneling from the n-type source electrode to the p-type drain electrode occurs via two localized states in the channel. These localized states (in a deep impurity and a shallow impurity) form a double quantum dot in which the spin qubit is formed in the spin-blockade regime. The g-factor of the spin can be tuned by the gate voltage, which enables the fast

modulation of the qubit energy. We demonstrated coherent control by modulating the qubit energy with various continuous waveforms. In particular, when modulated by asymmetric rectangular pulses with duty ratio d, we observed interferograms, which we refer to as weighted motional averaging. At low frequency, this displays d-weighted peaks which, at higher frequency, merge into one peak. To conclude, we summarize the advantages of the silicon single-spin interferometers: they operate at relatively high temperature (1.6 K), the g-factor is controlled by the gate voltage ($\sim 1\%$, important for selectivity of measurements), the relaxation times $T_{1,2}$ are large, the fabrication is based on the well-developed techniques for silicon, such as CMOS, and they can be manipulated into the ESR and Pauli spin blockade regimes.

Acknowledgments

We thank K. Ishibashi for discussions and M. Cirio and N. Lambert for critically reading the manuscript. This work was supported by JSPS KAKENHI Grant No. 15H04000, 17H01276. F.N. is supported in part by the MURI Center for Dynamic Magneto-Optics via the Air Force Office of Scientific Research (AFOSR) (FA9550-14-1-0040), Army Research Office (ARO) (Grant No. W911NF-18-1-0358), Asian Office of Aerospace Research and Development (AOARD) (Grant No. FA2386-18-1-4045), Japan Science and Technology Agency (JST) (Q-LEAP program and CREST Grant No. JPMJCR1676), Japan Society for the Promotion of Science (JSPS) (JSPS-RFBR Grant No. 17-52-50023 and JSPS-FWO Grant No. VS.059.18N), RIKEN-AIST Challenge Research Fund, and the John Templeton Foundation.

[1] B. P. Abbott *et al.* (LIGO Scientific Collaboration and Virgo Collaboration), "Observation of gravitational waves from a binary black hole merger," Phys. Rev. Lett. **116**, 061102 (2016).

[2] M. Suda, *Quantum Interferometry in Phase Space* (Springer, Berlin Heidelberg New York, 2006).

[3] D. Braun, G. Adesso, F. Benatti, R. Floreanini, U. Marzolino, M. W. Mitchell, and S. Pirandola, "Quantum-enhanced measurements without entanglement," Rev. Mod. Phys. **90**, 035006 (2018).

[4] S. Gerlich, S. Eibenberger, M. Tomandl, S. Nimmrichter, K. Hornberger, P. J. Fagan, J. Tüxen, M. Mayor, and M. Arndt, "Quantum interference of large organic molecules," Nat. Comm. **2**, 263 (2011).

[5] K. Hornberger, S. Gerlich, P. Haslinger, S. Nimmrichter, and M. Arndt, "Colloquium: Quantum interference of clusters and molecules," Rev. Mod. Phys. **84**, 157–173 (2012).

[6] W. D. Oliver, Y. Yu, J. C. Lee, K. K. Berggren, L. S. Levitov, and T. P. Orlando, "Mach-Zehnder interferometry in a strongly driven superconducting qubit," Science **310**, 1653–1657 (2005).

[7] M. Sillanpää, T. Lehtinen, A. Paila, Y. Makhlin, and P. Hakonen, "Continuous-time monitoring of Landau-Zener interference in a Cooper-pair box," Phys. Rev. Lett. **96**, 187002 (2006).

[8] S. N. Shevchenko, S. Ashhab, and F. Nori, "Landau-Zener-Stückelberg interferometry," Phys. Rep. **492**, 1–30 (2010).

[9] C. L. Degen, F. Reinhard, and P. Cappellaro, "Quantum sensing," Rev. Mod. Phys. **89**, 035002 (2017).

[10] J. J. L. Morton, D. R. McCamey, M. A. Eriksson, and S. A. Lyon, "Embracing the quantum limit in silicon computing," Nature **479**, 345–353 (2011).

[11] F. A. Zwanenburg, A. S. Dzurak, A. Morello, M. Y. Simmons, L. C. L. Hollenberg, G. Klimeck, S. Rogge, S. N. Coppersmith, and M. A. Eriksson, "Silicon quantum electronics," Rev. Mod. Phys. **85**, 961–1019 (2013).

[12] L. M. K. Vandersypen, H. Bluhm, J. S. Clarke, A. S. Dzurak, R. Ishihara, A. Morello, D. J. Reilly, L. R. Schreiber, and M. Veldhorst, "Interfacing spin qubits in quantum dots and donors–hot, dense, and coherent," npj Quantum Info. **3**, 34 (2017).

[13] R. Maurand, X. Jehl, D. Kotekar-Patil, A. Corna, H. Bohuslavskyi, R. Laviéville, L. Hutin, S. Barraud, M. Vinet, M. Sanquer, and S. De Franceschi, "A CMOS silicon spin qubit," Nat. Comm. **7**, 13575 (2016).

[14] M. F. Gonzalez-Zalba, S. N. Shevchenko, S. Barraud, J. R. Johansson, A. J. Ferguson, F. Nori, and A. C. Betz, "Gate-sensing coherent charge oscillations in a silicon field-effect transistor," Nano Lett. **16**, 1614–1619 (2016).

[15] K. Ono, G. Giavaras, T. Tanamoto, T. Ohguro, X. Hu, and F. Nori, "Hole spin resonance and spin-orbit coupling in a silicon metal-oxide-semiconductor field-effect transistor," Phys. Rev. Lett. **119**, 156802 (2017).

[16] M. P. Silveri, K. S. Kumar, J. Tuorila, J. Li, A. Vepsäläinen, E. V. Thuneberg, and G. S. Paraoanu, "Stückelberg interference in a superconducting qubit under periodic latching modulation," New J. Phys. **17**, 043058 (2015).

[17] M. P. Silveri, J. A. Tuorila, E. V. Thuneberg, and G. S. Paraoanu, "Quantum systems under frequency modulation," Rep. Prog. Phys. **80**, 056002 (2017).

[18] J. Li, M. P. Silveri, K. S. Kumar, J.-M. Pirkkalainen, A. Vepsäläinen, W. C. Chien, J. Tuorila, M. A. Sillanpää, P. J. Hakonen, E. V. Thuneberg, and G. S. Paraoanu, "Motional averaging in a superconducting qubit," Nat. Comm. **4**, 1420 (2013).

[19] J. Pan, Y. Fan, Y. Li, X. Dai, X. Wei, Y. Lu, C. Cao, L. Kang, W. Xu, J. Chen, G. Sun, and P. Wu, "Dynamically modulated Autler-Townes effect in a transmon qubit," Phys. Rev. B **96**, 024502 (2017).

[20] J. M. Fink, L. Steffen, P. Studer, L. S. Bishop, M. Baur, R. Bianchetti, D. Bozyigit, C. Lang, S. Filipp, P. J. Leek, and A. Wallraff, "Quantum-to-classical transition in cavity quantum electrodynamics," Phys. Rev. Lett. **105**, 163601 (2010).

[21] A. Fedorov, P. Macha, A. K. Feofanov, C. J. P. M. Harmans, and J. E. Mooij, "Tuned transition from quantum to classical for macroscopic quantum states," Phys. Rev. Lett. **106**, 170404 (2011).

[22] I. Pietikäinen, S. Danilin, K. S. Kumar, A. Vepsäläinen, D. S. Golubev, J. Tuorila, and G. S. Paraoanu, "Observation of the Bloch-Siegert shift in a driven quantum-to-classical transition," Phys. Rev. B **96**, 020501 (2017).

[23] J. Stehlik, Y. Dovzhenko, J. R. Petta, J. R. Johansson, F. Nori, H. Lu, and A. C. Gossard, "Landau-Zener-Stückelberg interferometry of a single electron charge qubit," Phys. Rev. B **86**, 121303 (2012).

[24] F. Forster, G. Petersen, S. Manus, P. Hänggi, D. Schuh, W. Wegscheider, S. Kohler, and S. Ludwig, "Characterization of qubit dephasing by Landau-Zener-Stückelberg-Majorana interferometry," Phys. Rev. Lett. **112**, 116803 (2014).

[25] J. Stehlik, M. Z. Maialle, M. H. Degani, and J. R. Petta, "Role of multilevel Landau-Zener interference in extreme harmonic generation," Phys. Rev. B **94**, 075307 (2016).

[26] M. Korkusinski, S. A. Studenikin, G. Aers, G. Granger, A. Kam, and A. S. Sachrajda, "Landau-Zener-Stückelberg interferometry in quantum dots with fast rise times: Evidence for coherent phonon driving," Phys. Rev. Lett. **118**, 067701 (2017).

[27] A. Bogan, S. Studenikin, M. Korkusinski, L. Gaudreau, P. Zawadzki, A. S. Sachrajda, L. Tracy, J. Reno, and T. Hargett, "Landau-Zener-Stückelberg-Majorana interferometry of a single hole," Phys. Rev. Lett. **120**, 207701 (2018).

[28] A. Chatterjee, S. N. Shevchenko, S. Barraud, R. M. Otxoa, F. Nori, J. J. L. Morton, and M. F. Gonzalez-Zalba, "A silicon-based single-electron interferometer coupled to a fermionic sea," Phys. Rev. B **97**, 045405 (2018).

[29] W. J. Pasek, M. Z. Maialle, and M. H. Degani, "Application of the Landau-Zener-Stückelberg-Majorana dynamics to the electrically driven flip of a hole spin," Phys. Rev. B **97**, 115417 (2018).

[30] J. V. Koski, A. J. Landig, A. Palyi, P. Scarlino, C. Reichl, W. Wegscheider, G. Burkard, A. Wallraff, K. Ensslin, and T. Ihn, "Floquet spectroscopy of a strongly driven quantum dot charge qubit with a microwave resonator," Phys. Rev. Lett. **121**, 043603 (2018).

[31] A. M. Ionescu and H. Riel, "Tunnel field-effect transistors as energy-efficient electronic switches," Nature **479**, 329–337 (2011).

[32] T. Mori, Y. Morita, N. Miyata, S. Migita, K. Fukuda, M. Masahara, T. Yasuda, and H. Ota, "Band-to-band tunneling current enhancement utilizing isoelectronic trap and its application to TFETs," in *VLSI Technology (VLSI-Technology): Digest of Technical Papers, 2014 Symposium on* (IEEE, 2014) pp. 1–2.

[33] T. Mori, W. Mizubayashi, Y. Morita, S. Migita, K. Fukuda, N. Miyata, T. Yasuda, M. Masahara, and H. Ota, "Effect of hot implantation on ON-current enhancement utilizing isoelectronic trap in Si-based tunnel field-effect transistors," Appl. Phys. Expr. **8**, 036503 (2015).

[34] T. Mori, Y. Morita, N. Miyata, S. Migita, K. Fukuda, W. Mizubayashi, M. Masahara, T. Yasuda, and H. Ota, "Study of tunneling transport in Si-based tunnel field-effect transistors with ON current enhancement utilizing isoelectronic trap," Appl. Phys. Lett. **106**, 083501 (2015).

[35] T. Mori, S. Iizuka, and T. Nakayama, "Material engineering for silicon tunnel field-effect transistors: isoelectronic trap technology," MRS Communications **7**, 541–550 (2017).

[36] K. Ono, T. Mori, and S. Moriyama, "High-temperature operation of a silicon qubit," Sci. Rep. **9**, 469 (2019).

[37] J. Weber, W. Schmid, and R. Sauer, "Localized exciton bound to an isoelectronic trap in silicon," Phys. Rev. B **21**, 2401 (1980).

[38] R. Sauer, J. Weber, and W. Zulehner, "Nitrogen in silicon: Towards the identification of the 1.1223-eV (A, B, C) photoluminescence lines," Appl. Phys. Lett. **44**, 440–442 (1984).

[39] R. A. Modavis and D. G. Hall, "Aluminum-nitrogen isoelectronic trap in silicon," J. Appl. Phys. **67**, 545–547 (1990).

[40] S. Iizuka and T. Nakayama, "First-principles calculation of electronic properties of isoelectronic impurity complexes in Si," Appl. Phys. Expr. **8**, 081301 (2015).

[41] See Supplemental Material at [URL will be inserted by publisher] .

[42] W. G. van der Wiel, S. De Franceschi, J. M. Elzerman, T. Fujisawa, S. Tarucha, and L. P. Kouwenhoven, "Electron transport through double quantum dots," Rev. Mod. Phys. **75**, 1–22 (2002).

[43] K. Ono, D. Austing, Y. Tokura, and S. Tarucha, "Current rectification by Pauli exclusion in a weakly coupled double quantum dot system," Science **297**, 1313–1317 (2002).

[44] F. H. L. Koppens, C. Buizert, K.-J. Tielrooij, I. T. Vink, K. C. Nowack, T. Meunier, L. P. Kouwenhoven, and L. M. K. Vandersypen, "Driven coherent oscillations of a single electron spin in a quantum dot," Nature **442**, 766–771 (2006).

[45] J. J. Pla, K. Y. Tan, J. P. Dehollain, W. H. Lim, J. J. L. Morton, D. N. Jamieson, A. S. Dzurak, and A. Morello, "A single-atom electron spin qubit in silicon," Nature **489**, 541–545 (2012).

[46] R. Rahman, S. H. Park, T. B. Boykin, G. Klimeck, S. Rogge, and L. C. L. Hollenberg, "Gate-induced g-factor control and dimensional transition for donors in multivalley semiconductors," Phys. Rev. B **80**, 155301 (2009).

[47] S. N. Shevchenko, A. S. Kiyko, A. N. Omelyanchouk, and W. Krech, "Dynamic behavior of Josephson-junction qubits: crossover between Rabi oscillations and Landau-Zener transitions," Low Temp. Phys. **31**, 569–576 (2005).

[48] O. V. Ivakhnenko, S. N. Shevchenko, and F. Nori, "Simulating quantum dynamical phenomena using classical oscillators: Landau-Zener-Stückelberg-Majorana interferometry, latching modulation, and motional averaging," Sci. Rep. **8**, 12218 (2018).

[49] L. Childress and J. McIntyre, "Multifrequency spin resonance in diamond," Phys. Rev. A **82**, 033839 (2010).